Synthesis of Charged Ultrafiltration Poly(styrene-*co*-divinyl benzene) Composite Membrane

Sonny Sachdeva, Anil Kumar

Department of Chemical Engineering, Indian Institute of Technology Kanpur, Kanpur 208016, Uttar Pradesh, India

Received 18 June 2007; accepted 4 April 2008
DOI 10.1002/app.28576
Published online 18 June 2008 in Wiley InterScience (www.interscience.wiley.com).

ABSTRACT: A ceramic supported crosslinked polystyrene composite membrane has been prepared from its monomers using a dual initiator system. The nonionic hydrophobic membrane so prepared has been chemically modified by a low temperature (50°C), single step reaction with chloroacetic acid. The carboxylated membrane has acid functional groups on its surface making it negatively charged and highly hydrophilic in nature. The membranes (unmodified and carboxylated) have been used for the separation of hazardous chromium (VI) salt solution where observed and intrinsic rejection has been studied as a function of pressure and concentration of the feed solution. The intrinsic rejection has been determined by calculating the concentration at the membrane surface (C_m) using Speigler-Kedam model and osmotic pressure model. The observed rejection for the chemically modified membrane decreases with increasing pressure but the intrinsic rejection is found to be more than 80% for all concentrations in the range of study. The experimental results have been fitted using Space-Charge model to obtain the membrane wall potential and the membrane surface concentration which are difficult to measure directly. The transport through the membrane capillaries has been described by the two dimensional model using Nernst-Planck equation for ion transport, Navier-Stokes equation and Poisson-Boltzmann equation for the radial distribution of potential. We have then presented a semianalytical series solution to the highly nonlinear Poisson-Boltzmann equation to reduce the computational time required to solve the set of coupled differential equations. The effective wall potential of the carboxylated membrane was found to be −28.07 mV. J Appl Polym Sci 110: 210–227, 2008

Key words: ultrafiltration membrane; concentration polarization; poly (styrene-*co*-divinyl benzene); space charge model; wall potential

INTRODUCTION

Development of new polymeric membrane materials and modification of the existing polymers for ultrafiltration is an area of constant interest in research. Membranes made from polymers like polystyrene,[1] polysulfone,[2] polytetrafluoroethylene,[3] polycarbonate,[3] polyethersulfone,[4] polypropylene,[5] etc. exhibit good mechanical and thermal properties but are hydrophobic in nature. Because of this reason, they give low water flux and are prone to fouling by adsorption of organic solutes. Membranes made from polystyrene and its copolymers have high chemical stability and mechanical strength and have been used for gas separation[1,6] as they are dense in nature requiring high operating pressures. Polystyrene membranes have been extensively used as ion exchange membranes as they can be easily functionalized. The sulfonated[7,8] and aminated membranes[9] have been used in electrodialysis, as proton exchange membranes in fuel cells[10,11] and as bipolar membranes.[12–14]

Correspondence to: A. Kumar (anilk@iitk.ac.in).

Journal of Applied Polymer Science, Vol. 110, 210–227 (2008)

In this work, we have reported a new way of preparing negatively charged carboxylated polystyrene membranes by introducing acid functional groups to the polymeric film supported on a ceramic support. Various methods have been reported in literature[15–17] for carboxylation of polystyrene. Styrene and maleic anhydride are copolymerized together and the anhydride group is hydrolyzed with NaOH to obtain acid functional groups on the membrane surface.[15] Polystyrene was also directly metallated using 1 : 1 mixture of butyllithium and potassium-*t*-butoxide in cyclohexane/hexane mixture.[16] The metallated polymer on reaction with solid carbon dioxide was carboxylated and further protonated by immersing in HCl solution. Carboxylated polystyrene latex particles have also been obtained by copolymerization of styrene with methacrylic acid using potassium persulfate as the initiator.[17]

Chromium can occur in several oxidation states (−2 to 6) of which only III and VI are naturally stable. Chromium is an essential nutrient for plant and animal metabolism but when accumulated at high levels (>0.1 mg/g body weight) in the human body can cause serious diseases like nausea, skin ulcerations, lung cancer, etc.[18] Chromium (VI), a highly toxic, carcinogenic oxidizing agent is a major effluent

from leather tanning, chromium electroplating, and chemical manufacturing industries[19] and its recovery is one of the major environmental problems. The most common method used for the recovery of chromium (VI) is chemical reduction of chromium (VI) to chromium (III), neutralization and precipitation at pH 7–9 followed by sedimentation and separation of metal hydroxides.[20] This method produces a large amount of sludge containing chemicals that cannot be used for the recycling of either chromium (VI) or water. The main disadvantages of this process are that it consumes large amount of reducing agents, increases the cost of treatment and long-term environmental damage. Various other technologies for removal of pollutant and recycling the water are ion exchange,[21,22] evaporation,[23] adsorption,[24] liquid–liquid extraction,[20,25,26] and membrane separation processes.[27–33]

In this article, we have prepared ceramic supported poly(styrene-*co*-divinyl benzene) (PS) composite membrane using a dual initiator (azobis-isobutyronitrile (AIBN), benzoyl peroxide (BPO) system catalyzed by *N,N*,-Dimethyl Aniline (DMA) which gives stable polymer syrup in its own monomer. This is further used in preparing a thin crosslinked ultrafiltration membrane on a ceramic support. The membranes so prepared are further modified by reaction with chloroacetic acid. The membranes prepared in this way have high water flux at very low pressure drop without much loss in rejection of the solute (chromium VI). The membranes have been fully characterized using Scanning Electron Microscopy (SEM), Fourier Transform infrared spectroscopy (FTIR), Atomic Force Microscopy (AFM), contact angle measurements, water content, and molecular weight cut off experiments. Here, the separation performance of the membrane so prepared has been evaluated by utilizing it for the removal of harmful chromium (VI) for a range of feed concentrations as a function of pressure. The separation is carried out using charged membranes and therefore we have obtained the real rejection of chromium (VI) more than 80% even for very low concentrations.

Space Charge Model (SCM) has been used to fit the experimental results to determine membrane wall potential and surface concentration which are difficult to measure directly. The SCM uses Nernst-Planck equation to determine the flux of ions, Navier-Stokes equation to determine the fluid dynamics (bulk velocity/volume flow) and Poisson-Boltzmann equation to relate the distribution of electrical potential to space charge density (concentration profile of solutes). In the experimental data fitting, it was observed that the numerical solution of nonlinear Poisson-Boltzmann equation (PBE) had to be integrated several times which took a large amount of computation time (of the order of 15 h). To overcome this problem, we have developed a series solution of the nonlinear Poisson-Boltzmann differential equation which leads to considerable saving of computation time.

TABLE I
Composition of Clay Supports

Clay raw material	Chemical formula	Composition (wt %)
Kaolin	$Al_2(Si_2O_5)(OH)_4$	13.28
Ball clay	$3SiO_2.Al_2O_3$	16.15
Feldspar	$(Na, Ca)(AlSi_3O_8)$	5.15
Quartz	SiO_2	24.44
Pyrophyllite	$Al_2(Si_2O_5)_2(OH)_2$	13.54
Calcium carbonate	$CaCO_3$	27.44

EXPERIMENTAL

Materials

Analytical grade calcium carbonate, chromium trioxide, BPO, and azobis-isobutyronitrile (AIBN) are procured from S.D. Fine Chemicals, (Bombay, India). Analytical grade tetraethylorthosilicate (TEOS), dimethylaniline (DMA), polyethyleneglycol (PEG), sodium hydroxide, hydrochloric acid, toluene, methanol, and fused calcium chloride are obtained from Qualigens, Bombay. Styrene and divinyl benzene (DVB) are obtained from Merck (Philadelphia).

Before polymerization, styrene and DVB are first washed with 5% NaOH solution and then vacuum distilled to remove all the inhibitors. AIBN and BPO are recrystallized in methanol before being used as initiators for styrene-DVB polymerization reaction. All the other chemicals are used as received.

Preparation of clay supports

An integral part of the composite membranes is the support which provides sufficient mechanical and chemical strength to the membrane. In this work, we have used a clay support for the preparation of composite membrane. The support is prepared from a mixture of different clays (kaolin, ball clay, pyrophallite, calcium carbonate, feldspar, and quartz) in the composition given in Table I.[34] A homogeneous paste of all these clays is made in distilled water and cast on a gypsum surface using an aluminum ring of 76 mm internal diameter and 4 mm thickness. The supports are dried at room temperature, 100 and 250°C for 24 h each to ensure slow removal of water. After the complete drying of the supports, they are calcined at 900°C in the furnace for 8 h to impart the required mechanical strength and porosity. Finally, the calcined supports are polished on a silicon abrasive paper (No. C-220) to get smooth and flat clay discs of 64 mm diameter and 2–3 mm thick-

ness. To increase the stability of the membrane in oxidizing and reducing environments the finished supports are dipped in a solution of TEOS, which is prepared at room temperature by continuous stirring of TEOS, HCl, and water in the molar ratio of 1 : 0.04 : 2. Subsequently, the TEOS dipped clay supports are calcined at 1000°C for 5 h.

Preparation of crosslinked carboxylated polystyrene composite membrane

Preparation of polystyrene membrane

The composite poly(styrene-*co*-divinyl benzene) membranes were prepared by first preparing a homogeneous copolymer solution in toluene and then coating it uniformly on the wet clay support. The homogeneous copolymer solution is prepared by polymerizing its monomers styrene and DVB, using a dual initiator system (BPO and AIBN) in the presence of DMA. Here DVB also acts a crosslinking agent. In a typical experiment, a mixture of styrene (0.1344 gmole), DVB (3.22×10^{-3} gmole), AIBN (6.308×10^{-4} gmole), and BPO (7.64×10^{-4} gmole) with DMA (0.057 g, 4.70×10^{-4} gmole) is heated and stirred in N_2 atmosphere at 70°C for 1 h in an oil bath and then cooled to room temperature quickly by placing the mixture in a refrigerator to arrest the further progress of the polymerization reaction. The reaction is continuously monitored and the monomer conversion is checked at regular intervals of time. The cooled reaction product, which is a homogeneous solution of the copolymer (10% conversion of the initial weight of the monomers), is diluted with toluene to 66% by weight of copolymer under continuous stirring so as to remove any bubbles present in the solution. The presence of bubbles in the copolymer solution leads to formation of pinholes on the membrane surface after it is casted on the clay support.

The clay support is placed over wet polyurethane foam to displace the air present inside the supports by water. Approximately 2 g of the polymer solution is poured and uniformly spread on the wet clay and dried overnight at room to evaporate all the solvent (toluene). During the casting of the polymer solution on the clay support, the support is wet kept primarily for two reasons. First, to remove the air present in the microporous clay support and second to stop the polymer from penetrating inside the clay support. Since water is a nonsolvent for the copolymer solution it does not allow the polymer to seep inside the pores of the clay support forming a thin, distinct layer on its surface. The polymer coated clay support thus formed is finally crosslinked by vacuum heating at 70°C for 12 h. The amount of uncrosslinked polymer was determined by leaching the membrane material with solvent, toluene and determining the change in the mass of the material after leaching. The amount of crosslinked polymer in the membrane was thus found to be about 85%. However, experiments have shown that the linear polymer is extremely entangled with the crosslinked polymer and there is no change in dimension on application of pressure. All our experimental results on separation show no hysteresis. In the following sections, we will denote the polymer coated clay support as ''composite membrane.''

Modification of polystyrene clay composite membrane

The polystyrene composite membrane so prepared is nonionic and hydrophobic in nature which needs to be chemically modified to make it charged and hydrophilic. We have carried out surface modification of the polymer film of the composite membrane to obtain a negatively charged membrane having carboxylic acid functional groups on its surface. The composite membrane is treated with a 30% (by vol.) solution of chloroacetic acid ($CClH_2COOH$) in distilled water for about 6 h at 50°C in a glass reactor. After the reaction, the membrane is washed thoroughly with distilled water to remove the unreacted acid on the membrane. The membrane is further treated with 10% (by wt.) NaCl solution at 50°C for 4 h to transform it into ionizable form. The membrane before the modification was transparent and glossy whereas after modification it became pale and matte in appearance. The modified membrane is referred to as carboxylated membrane (CM) from hereon in the rest of the text.

Characterization of carboxylated membrane

Scanning electron microscopy

Scanning electron microscope (SEM) (Joel-JSM, Model 840 A) at 3 keV acceleration has been used to analyze changes in the structural morphology of the CM after chemical modification. SEM pictures of the top surface and the cross-sectional area of the unmodified membrane (UM) and CM are obtained at 10 K and 26 K magnifications. The membrane samples are dipped in liquid nitrogen and sputtered with gold to a thickness of approximately 150 Å to create a conducting surface, before being analyzed.

Atomic force microscopy

Atomic force microscope (AFM) is an advanced characterization tool which has been applied extensively for studying ultrafiltration and nanofiltration membranes. AFM has eliminated the tedious process

of sample preparation as it can image nonconducting samples and is used to determine the average pore size and surface roughness of the membrane. All the samples were scanned using Molecular Imaging (MI), made AFM equipment in Acoustic AC (AAC) mode. Advantage of AAC mode is that the phase image is also obtained with topographic image. A sharp cantilever tip scans the surface of the membrane and generates a line profile of the surface. Cantilevers used for AAC mode NSC 12I are from Mikro Masch having force constant $\sim$ 4.5 N/m and frequency $\sim$ 150 kHz. All the samples are imaged at various scan area of 30×30 μm^2, 10×10 μm^2, and 5×5 μm^2 and at different locations of the sample. The scan speed is kept around 2 lines/s and the imaging is done in air at room temperature. The line profiles obtained are used to estimate the pore sizes of the membranes.

Pore sizes are measured by visual inspection of line profiles of various AFM images of different areas of the same membrane. These pore sizes are then arranged in ascending order and assigned median ranks. Median ranks are calculated from the following formula.

$$\text{median} = \frac{j - 0.3}{n + 0.4} \times 100 \quad (1)$$

where j is the order number of the pore when arranged in ascending order and n is total number of pores measured.[35]

To obtain a cumulative distribution function graph, these median ranks are plotted on the ordinate axis against pore sizes arranged in an increasing order on the abscissa. This plot yields a straight line on a lognormal probability paper if the pore sizes have a lognormal distribution. From this graph, values of mean pore size (μ_p) can be calculated.

Molecular weight cut off

The molecular weight cut-off (MWCO) of the membranes is determined by analyzing the rejection of 1000 ppm solution of polyethylene glycol (PEG) of different molecular weight (200–35,000 Dalton). All the experiments are conducted at room temperature and at 275.7 kPa. The membranes are compacted at a pressure (482 kPa) higher than the operating pressure (275.7 kPa) for 5 h before any measurement. The concentration of PEG in the feed and permeate is estimated using refractive index (RI) measurements. The pore diameter of the membrane is determined using the following equation[35]

$$a = 16.73 \times 10^{-10} M^{0.557} \quad (2)$$

where, a is the pore radius of the membrane in cm, M is the molecular weight cut-off of the membrane.

Fourier transform infrared spectroscopy

To identify the carboxylic acid functional groups introduced by the chemical modification on the UM, the FTIR spectra of the unmodified and modified unsupported polystyrene films are obtained using Bruker VERTEX 22 spectrometer in the range of 500–4000 cm^{-1}. The spectra are obtained by making a pellet of 1 mg powder of crushed polymer films as samples and 200 mg of IR spectroscopic grade KBr pellets.

Cation exchange capacity

Cation exchange capacity (CEC) is an important electrochemical property of charged membranes and is a measure of number of fixed charges per unit weight of dry membrane. To determine CEC, the carboxylated polystyrene film is first immersed in distilled water for a period of 24 h and then in 1*N* HCl aqueous solution for another 24 h to convert it to H^+ forms. The film is washed with distilled water to remove excess of acid and finally equilibrated with 0.5*N* NaOH aqueous solution for 24 h. Cation exchange capacity (mequiv/g) is determined from the reduction in alkalinity by back titration using the following equation[36]

$$\text{CEC} = (N_1 - N_2) \times V/W \quad (3)$$

where, N_1 is the normality of NaOH before equilibration in mol/L, N_2 is the normality of NaOH after equilibration in mol/L, V is the volume of NaOH taken for titration in ml, and W is the weight of modified PS film in g.

Contact angle measurement

Sessile drop method is used to measure the contact angle of the UM and CM. Static contact angles of the membrane surface with water are measured using a Goniometer (Model 100-00-230) supplied by r'amehart with RH1 2001 Imaging software. Measurements are carried out on unmodified and modified polystyrene composite membranes to confirm the effect of modification on the hydrophillicity of the membrane. Droplets of double distilled water ($\approx$3 mL) are positioned at different places and at least 20 readings are taken to determine the average values.

Equilibrium water content

The water content of the membranes (only polymer films) has been measured by calculating the difference in weight of the dry and wet membrane sample. The unmodified and carboxylated unsupported polymer films are completely soaked in water for 24 h to ensure saturation. The excess water is

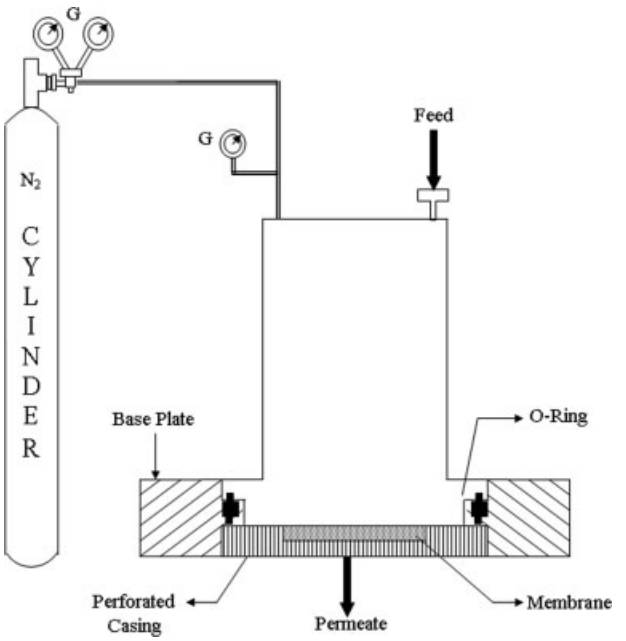

Figure 1 The schematic representation of the unstirred batch ultrafiltration experimental setup where G represents the pressure gauge.

removed by gently wiping it off with a filter paper and the wet membrane samples are weighed. These are then dried at 60°C to completely remove the water and weighed again till a no change in the weight is obtained.

$$\text{Water Uptake}\,(\%) = \frac{W_{\text{wet}} - W_{\text{dry}}}{W_{\text{dry}}} \times 100 \qquad (4)$$

Experimental set up for ultrafiltration

Ultrafiltration experiments have been conducted in dead end type laboratory test cells each having an effective area of 40 cm^2. The batch cell (Fig. 1) consists of two parts, cylindrical top part and a base plate made of stainless steel SS316 having a height of 240 mm and an outer diameter of 76 mm. The base plate has circular groove of 4 mm depth, which houses the membrane. The ceramic composite membrane is placed inside a perforated stainless steel casing of 60 mm inner diameter and 2–3 mm deep grooves. The membrane cast in a steel casing sealed with a fast-setting epoxy resin is placed inside the cylindrical groove of the base plate. The upper half of the cell is fixed to the base plate by nut and bolt and an *o*-ring is kept on the membrane to make the entire setup leak proof. The membrane cross-sectional area available for flux and retention measurements is 36 cm^2. The test cells have an inlet in the top part to fill the cell with feed solution and an outlet at the bottom to collect the permeate. The cell is pressurized from the N_2 cylinder and the pressure applied is measured using a gauge.

The membrane is compacted with double distilled water at a pressure (482 kPa) higher than the maximum operating pressure till a constant water flux is obtained. Pure water flux and permeate flux have been obtained by measuring the time required to collect 25 mL permeate volume. Before each run, the membrane is cleaned with distilled water at higher pressure (482 kPa) and water flux is determined to ensure that there is no flux decline due to partial plugging. For each run the cell is filled with 500 mL of feed solution and permeate flux is measured after 50 mL of permeate passed through the membrane.

We have carried out the separation experiments with chromium (VI) salt solution and its concentration in the feed and permeate is measured by a conductivity cell (Century CMK 731, μP based water analysis kit) with 0.1 μS accuracy and a UV spectrophotometer (Elico SL159) at 372 nm. All calibration curves (conductivity versus concentration and absorbance versus concentration) were linear in the range of concentrations used (10–1000 ppm). The separation experiments have been conducted at five different pressures (68–300 KPa) and three different initial concentrations of chromium (VI) (100–1000 ppm) at pH = 3.

Permeate flux and intrinsic rejection

The pure water flux through an ultrafiltration membrane can be described by the Darcy's law, which states that volumetric flux is directly proportional to the applied pressure gradient.

$$J_w = K\Delta P_{\text{applied}} \qquad (5)$$

where $K = 1/R_m\mu_w$, R_m = Intrinsic hydraulic resistance, J_w = Water flux, μ_w = Viscosity of water.

In ultrafiltration experiments, the rejection factor is defined as

$$R_{\text{obs.}}\,(\%) = \left(1 - \frac{C_P}{C_R}\right) \times 100 \qquad (6)$$

$$R_{\text{int.}}\,(\%) = \left(1 - \frac{C_P}{C_m}\right) \times 100 \qquad (7)$$

where C_P = Solute concentration in permeate, C_R = Solute concentration in retentate (in bulk), C_m = Solute concentration at the membrane interface, R_{obs} = Observed rejection factor, R_{int} = Intrinsic rejection factor.

Intrinsic rejection is an inherent property of the membrane which includes concentration polarization effects whereas observed rejection depends strongly

on the operating conditions. It is therefore desirable to report separation performance of a membrane in terms of the former, even though the direct measurement of solute concentration at the membrane surface (C_m) done through interoferometric[37,38] and optical shadow measurements[39] is difficult. C_m can also be determined indirectly by solving transport equations in the polarization layer. Accuracy of the estimated C_m depends on the validity of the hydrodynamic model used.

The membrane surface concentration is calculated using the osmotic pressure model[38]

$$J_v = L_p(\Delta P - \sigma\Delta\pi) \tag{8}$$

where J_v is the permeate flux, ΔP, the applied pressure difference, σ, the membrane reflection coefficient and $\Delta\pi$, the osmotic pressure difference. The osmotic pressure difference is calculated using the van't Hoff equation for electrolytes.

$$\Delta\pi = vRT\Delta C \tag{9}$$

The reflection coefficient is related to the intrinsic rejection of the membrane through the equation given by Spiegler and Kedem.[40]

$$R_{\text{int}} = \sigma(1 - F)/(1 - \sigma F) \tag{10}$$

where F is given by

$$F = \exp\{-(1 - \sigma)J_v/P_m\} \tag{11}$$

The C_m, σ, and P_m (solute permeability) are calculated using eqs. (8)–(11) following the iterative technique given by Ghose et al.,[41] with the convergence criterion being a change of less than 2% in the value of surface concentration of the membrane (C_m).

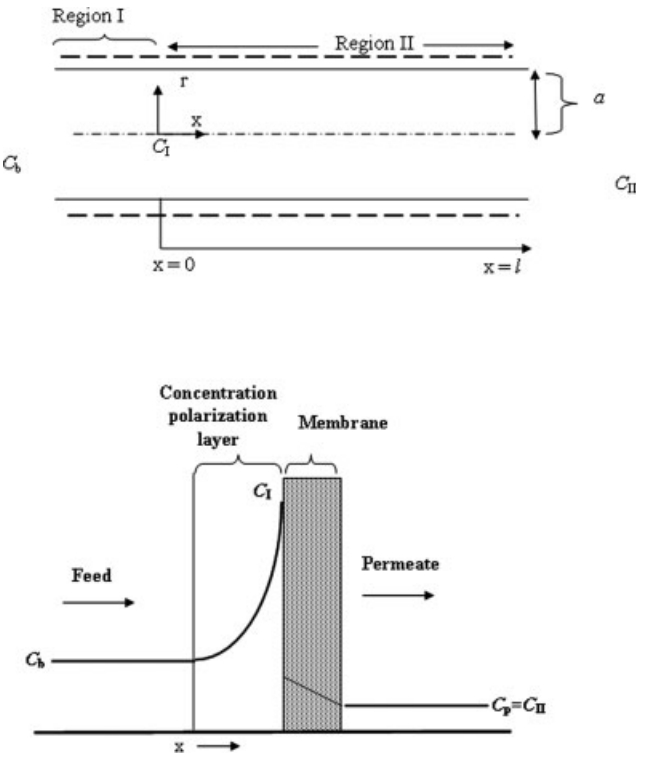

Figure 2 (a) The representation of a negatively charged cylindrical pore in the ultrafiltration membrane (b) Schematic view of the membrane showing the concentration profile of the solute in the bulk, concentration polarization layer and membrane.

Space charge model

In this work, we have separated chromate anions from its solution by using negatively charged membranes on the application of pressure. Charged porous membranes have a charge distributed on the surface as well as inside the pores which is not possible to measure directly. When an electrolyte comes in contact with a charged membrane pore an electrical double layer develops within it giving rise to a radial variation of the electrical potential and an unequal distribution of the cations and anions. This results in the development of a nonzero space charge region causing a coupling of electrical forces, mass transfer, and fluid flow. Therefore, an estimation of the effective wall potential which characterizes a charged membrane is of great importance. In view of this, the effective wall potential of the membrane has been found by fitting the experimental results using Space charge model (SCM).

In the model, the membrane is assumed to consist of a collection of long, narrow, parallel cylindrical capillaries carrying a uniformly distributed electrical surface charge. The length the pores, l, is relatively large as compared with the radius, a ($l \gg a$) as shown in Figure 2(a) (schematic of a single capillary). The electrolyte concentrations in the feed and permeate solutions, that is, at either end of the pore are denoted as c_b (upstream concentration) and c_p (downstream concentration), respectively, as shown in Figure 2(a). We use cylindrical coordinate system (r, θ, x) with x being positive in the direction of decreasing solute concentration. It is further assumed that the ion concentrations and electrical potentials are invariant in θ-direction of the pores.

In our model, we have assumed the membrane capillary to be divided into two regions. In the first region (Region I), increase in concentration occurs from c_b to c_I due to the unstirred concentration polarization layer [Fig. 2(b)] and the interfacial resistance of the membrane. Since, it is difficult to

measure c_I directly we have fitted it as a parameter to match the pressure Peclet number (Pe_p) and Peclet number (Pe). The Region II corresponds to the part of the membrane capillaries where the SCM holds well and describes the effect of wall potential on the movement of ions. The concentrations at the pore mouth and tail of the pore are c_I and c_{II} respectively, and c_{II} is taken to be equal to c_p.

The SCM uses Nernst-Planck equation [eq. (A1) of appendix A] to determine the flux of ions, Navier-Stokes equation [eq. (A2) of appendix A] to determine the fluid dynamics (bulk velocity/volume flow) and Poisson-Boltzmann equation [eq. (A4) of appendix A] to relate the distribution of electrical potential to space charge density (concentration profile of solutes). The basic governing equations describing the flow of chromium (VI) solution through the pore (momentum, convective-diffusion and Poisson-Boltzman equations) are presented in the Appendix A. It may be noticed that the system of governing equation represents a set of coupled nonlinear differential equation and they have to be solved simultaneously. All the equations are written in nondimensionalized form and for the nondimensionalization of concentration, c_I and solute flux J_s, we have taken the permeate concentration (c_{II}) instead of the upstream concentration (c_I), as done by Sasidhar and Ruckenstein[42]). On doing this, it can be easily seen that the ratio J_s^*/Pe is equal to 1 which leads to incorporation of the concentration polarization effects in a natural way and also simplifies the computation scheme.

The Poisson-Boltzman equations have been solved using a series solution.[31] To solve eq. (A4) semi analytically, we write potential ($\bar{\psi}$) in the form of an infinite power series.

$$\bar{\psi} = \sum_{i=0}^{\infty} a_i \eta^i \tag{12}$$

Substituting this in eq. (A5a), to satisfy the first boundary condition of Poisson-Boltzmann equation one sees that

$$a_1 = 0 \tag{13}$$

Substituting eq. (12) into the Poisson-Boltzmann, eq. (A4) we obtain

$$\sum_{i=0}^{\infty} (i+2)^2 a_{i+2} \eta^i = \frac{1}{\lambda^2} \sum_{i=0}^{\infty} \frac{\bar{\psi}^{2i+1}}{(2i+1)!} \tag{14}$$

Substituting eq. (12) into the RHS of the above equation, we obtain expressions for a_i by comparing the coefficients of η^i on both sides. These a_i's are dependent on a_0 and have been given in the appendix Table A1. The coefficient a_0 is the only independent coefficient andcan be determined from the second boundary condition A5b as follows.

$$\sum a_i = \psi_w \qquad \text{at } \eta = 1 \tag{15}$$

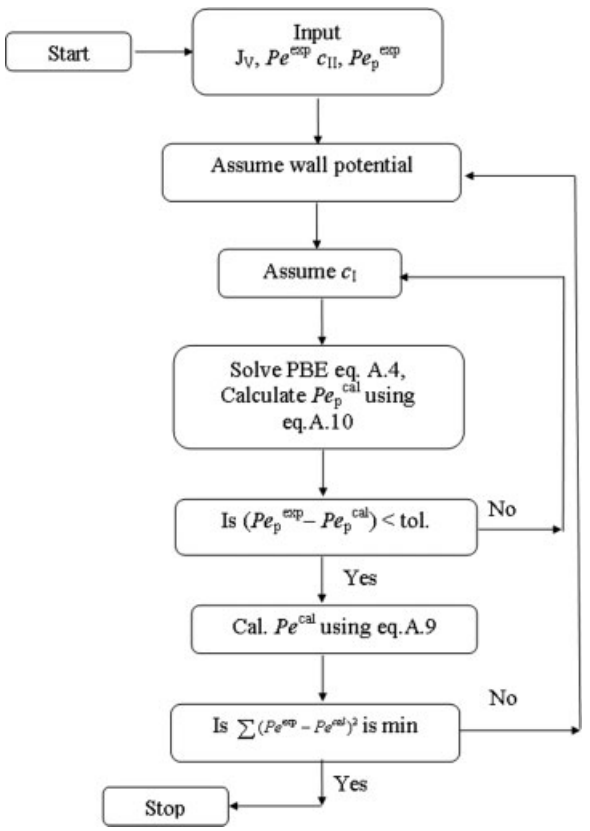

Figure 3 Algorithm for simulation of space charge model for separation of chromium (VI) salt solution.

Another computationally intensive part of the SCM is the evaluation of the integrals k_0 to k_9 (given in Table A2) used for calculation of parameters L_1 to L_4 in eq. (A8). We have obtained analytical expressions for these integrals by using the series solution of Poisson-Boltzmann equation and have been given in Table A2. In Ref. 42, the integrals k_0 to k_9 have been solved numerically but we have given analytical expressions for the same. We have matched our results obtained using series solution with the numerical results.

Here, the objective of fitting the experimental results obtained from ultrafiltration experiments is to characterize our membrane in terms of effective wall potential and the determination of c_I to calculate the rejection obtained from SCM. The solution scheme is given in Figure 3 and can be described as follows: The available experimental data include permeate flux (J_v or Pe^{exp}), permeate concentration (c_{II} or J_s) and the applied pressure difference (Pe_p^{exp}). It may be noticed that the model uses the concentration of solute at the membrane surface (c_I) which is not the

same as the bulk concentration (c_b) of the retentate (i.e., available from experiments) because of the concentration polarization effects. The concentration at the membrane surface is therefore considered as one of the unknown variables that has to be determined from the solution of the model equations. The solution of equations is used to determine the effective wall potential of the pores as shown below.

The algorithm (given in Fig. 3) starts with the input of the experimental data ($Pe^{\exp}$, $Pe_p^{\exp}$ and c_{II}). A value of wall charge or wall potential is assumed and for each of the experimental data (c_{II}), a surface concentration (c_I) is first assumed and applied pressure difference (Pe_p^{cal}) is calculated by solving Poisson-Boltzmann equation [eq. (A4) of appendix A] and eq. (A10) of appendix A. If Pe_p^{cal} is not sufficiently close to the experimental value $Pe_p^{\exp}$, a new value of the c_I is assumed till the calculated value of Pe_p^{cal} is within the tolerance limit of the experimental value. Once c_I has been determined, the Peclet number (Pe^{cal}) is calculated for each set of experimental data using eq. (A9) of the appendix A. The sum of the squares of the difference in the calculated and experimental values of the Peclet number ($\sum (Pe^{\exp} - Pe^{cal})^2$) is determined. This exercise is repeated for different values of wall potential till a minimum value of the error is obtained and is taken as the effective wall potential of the pores.

The physical data that the model uses diffusion coefficients of the ions (D_i), Faraday's constant (F), universal gas constant (R), temperature (T), dielectric constant (ε_0), and dynamic viscosity of the water (μ). The bulk diffusion coefficient values in water are used in this study and are determined from the data of equivalent conductance of ions at infinite dilution as given in the literature.[43] In addition to these, the model requires characteristic membrane structural (pore radius, membrane area, and pore length). Of these, total cross-sectional area of the pores can be reasonably well estimated by determining the top surface area and porosity of the membrane. The pore length has been determined from the cross-sectional SEM photographs of the membranes.

RESULTS AND DISCUSSION

Development of clay supports

The microporous clay supports prepared in this work have good mechanical and chemical stability. During calcination the supports gain sufficient strength and hardness. However, if the supports are dried nonuniformly or differentially they are liable to crack. Hence, slow drying of the supports is of prime importance. These supports have been casted on a gypsum surface specifically as it absorbs water instantaneously from the support while if they are casted on a glass or steel surface they crack immediately as they do not absorb the water. Even after taking all the precautions to get flat supports, defects like surface nonuniformity would crop up after calcination. The surface nonuniformity, thus introduced, is removed by polishing the sintered clay discs on a fine silicon carbide abrasive paper (No.C-220). Sintering the supports after dipping in TEOS makes them more chemical resistant and they can withstand harsh oxidizing and reducing atmosphere for longer periods of operation. When used in the ultrafiltration experiments, they were found to be unaffected by the oxidizing effect of chromium (VI) salt solution.

Preparation of crosslinked carboxylated polystyrene composite membrane

The preparation of the polymer composite membrane includes two steps: First, preparation of a viscous polymer solution of monomer conversion 10% and second, casting of the polymer solution on the clay support and further crosslinking the polymer. In both the steps of preparation, it is required that the polymerization reaction should proceed continuously so as to obtain a high molecular weight polymer membrane. Here, we have copolymerized styrene and DVB using a dual initiator system of AIBN and BPO in the weight ratio of 1 : 2 in presence of DMA accelerator because DMA forms a radical cation with BPO.[44] This radical cation has considerably high reactivity and its activation energy is much lower than that of the dissociation of BPO and therefore causes the polymerization to progress even at room temperature while the casting and drying of he membrane. The AIBN initiator alone decomposes to its radicals at higher temperature of 50–70°C and is unaffected by the room temperature polymerization. If a mixture of BPO and DMA initiator system (without AIBN) alone is used, we find that on further heating the polymerization does not progress anymore (monomer conversion 8%) and we obtain a very low molecular weight membrane. However, on using dual initiator system of BPO and AIBN in presence of DMA, the monomer conversion stops at 10% (after 1 h reaction at 70°C), progresses further at room temperature slowly while casting because of BPO + DMA radical and on further heating to 70°C the polymerization is found to progress to completion due to AIBN. After crosslinking for 12 h, we determined the fraction of crosslinked polymer in the membrane to be about 85%. This is because, we have taken a low (3 wt %) of DVB because a high percentage of divinyl benzene (DVB) would give a highly crosslinked membrane which would swell very little in the solvents in which it is to be chemically modified. As a result of this, the polymer does not get fully functionalized and has low ion

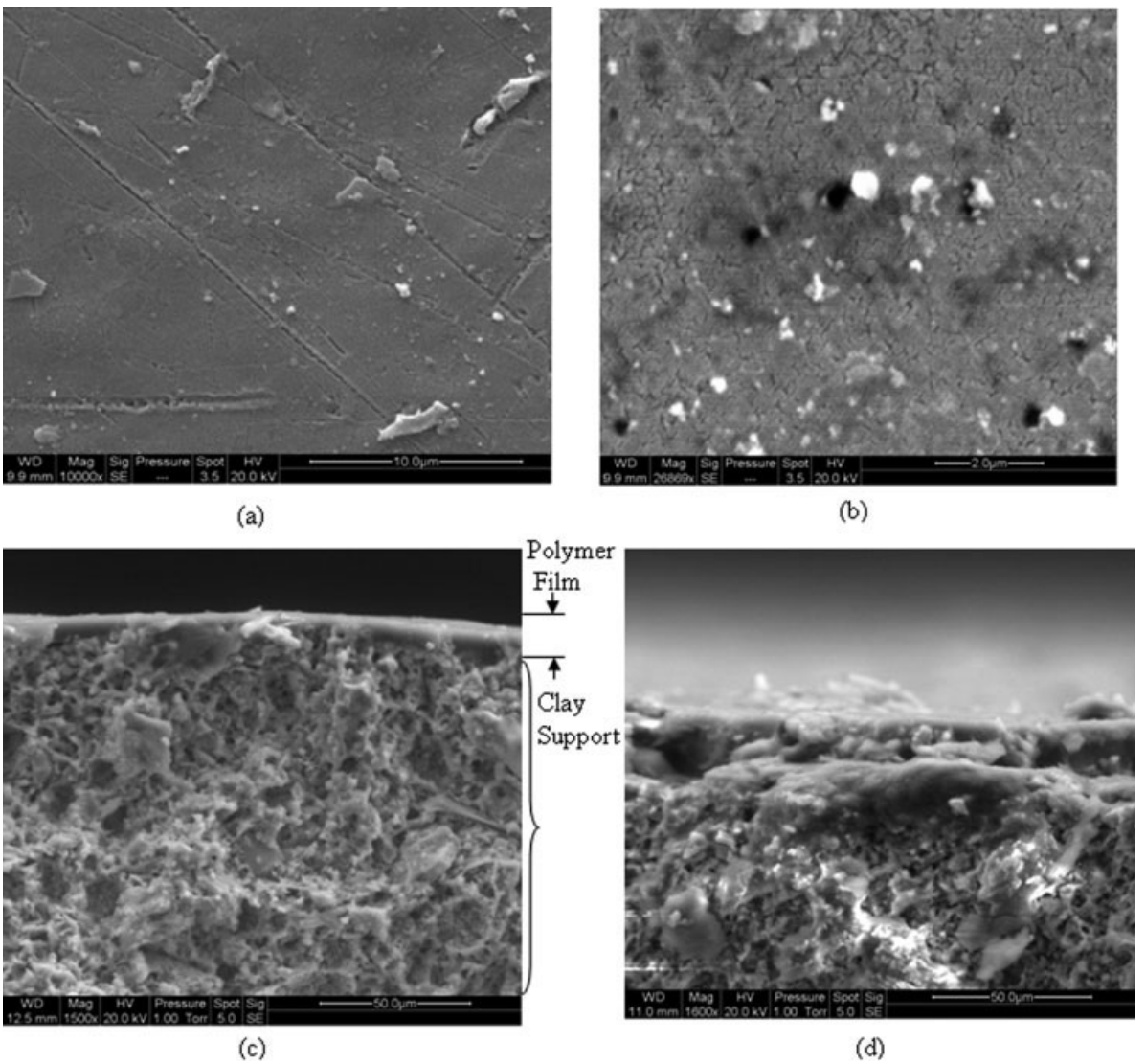

Figure 4 (a) SEM picture of unmodified membrane (UM) showing the cleavages on the membrane surface which are superficial (b) Carboxylated membrane (CM) in which black spots appear to be the pores (c) cross-sectional view of the membrane unmodified membrane (d) cross-sectional view of the modified membrane.

exchange capacity. However, experiments have shown that the linear polymer is extremely entangled with the crosslinked polymer and there is no change in dimension on application of pressure and all our experimental results on separation showed no hysteresis.

The composite membrane so prepared has been modified by reaction with chloroacetic acid to introduce carboxylic acid functional groups on its surface. As discussed in the previous section, a number of ways have been reported to do the same but the method developed in this work is advantageous as it is a low temperature, single step procedure, and the acid functional groups can be introduced uniformly into the polymer chain making the membrane charged and hydrophilic.

Characterization of carboxylated membrane

The main aim of the characterization of the membrane is to determine the relationship between the surface properties and the separation properties.

Scanning electron microscopy

The SEM pictures of the UM and CM are shown in Figure 4. In Figure 4(a), a smooth layer of UM at 10 K magnification is clearly visible with lines running across the surface. These lines on higher magnifications show a cleavage due to evaporation of solvents, but since pressure is required to cause a flow across the membrane, it is concluded that these cracks are superficial and the membrane material is

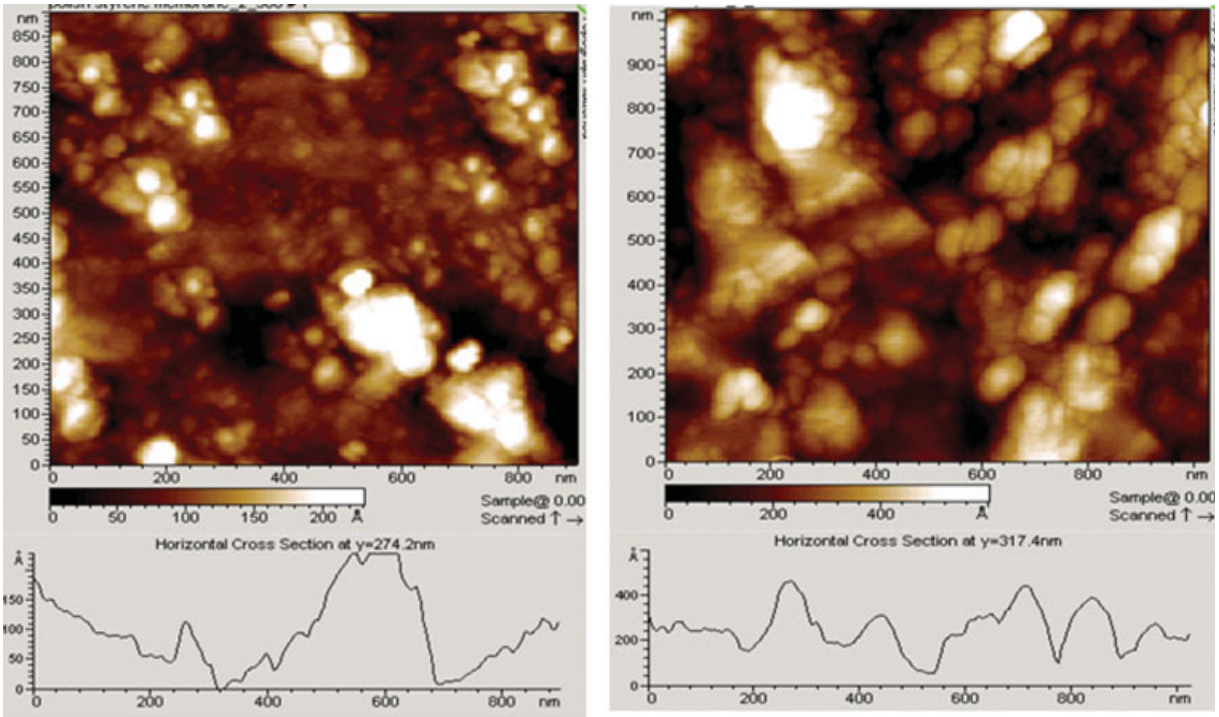

Figure 5 AFM image of (a) Unmodified membrane (UM) (b) Carboxylated membrane (CM) where the darker regions represent the pores. [Color figure can be viewed in the online issue, which is available at www.interscience.wiley.com.]

continuous. The SEM picture of the modified membrane is shown in Figure 4(b) at the magnification of 26 K. One can clearly see the development of pores on the membrane surface as a result of the modification with chloroacetic acid. The reaction of the polymer film with chloroacetic acid not only modifies it chemically but also causes an etching on the membrane surface which leads to the formation of pores. The cross-sectional view of the membrane [see Fig. 4(c)] shows a distinct layer of the polymer film on the clay support without any penetration of the polymer inside the clay supports. We have also shown the cross-sectional view of the modified membrane in Figure 4(d).

Atomic force microscopy

The images obtained by AFM have different pore shapes including circular, elliptical, and slits and the pore sizes have been calculated by taking an average of the length and width of the pore. The AFM images of the UM and modified membrane are shown in Figure 5. The bright regions correspond to the highest points and the dark regions are the pores. We have obtained line profiles of about 35 different pores by the visually inspecting the AFM images of different areas of the same membrane. The median ranks are plotted against pore sizes arranged in an increasing order on a lognormal probability paper which yielded a straight line confirming that the pores have a log normal distribution. Values of the mean pore size have been calculated from the data plotted which are found to be 30 and 39 nm for the UM and CM, respectively. The cumulative distribution curve is also obtained and is shown in Figure 6. The pore sizes obtained from AFM are much larger than those obtained from MWCO as the former measures the size of surface pores but the latter gives the actual pore size of the maximum number of pores present on the membrane surface.

Molecular weight cut-off of the membrane

The molecular weight cut for the UM and CM, as shown in Figure 7, have been determined to be 12,000 and 18,000 Dalton that correspond to average pore diameters of 6.3 and 7.8 nm [calculated from eq. (2)], respectively. This establishes the fact that they are ultrafiltration membranes and that the modification reaction causes an increase in the pore size (MWCO) of the CM.

FTIR spectroscopy

The FTIR analysis has been carried out to confirm the presence of carbonyl (C=O) functional groups, characteristic of carboxylic acid, on the modified membrane surface. The FTIR spectra of the UM and

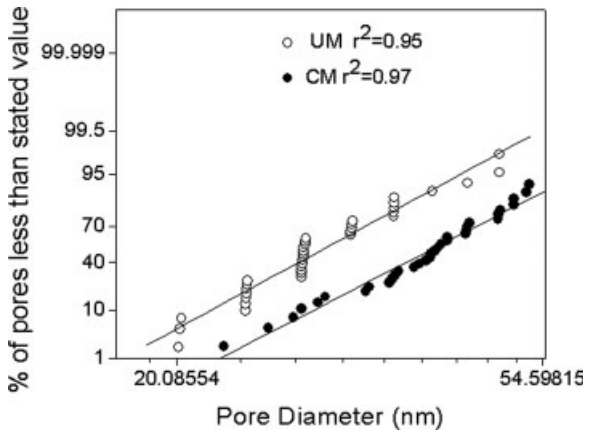

Figure 6 Log-normal pore size distributions of the pore sizes of unmodified (UM) and carboxylated (CM) membranes measured from AFM images.

modified membrane obtained in the range of 4000–500 cm^{-1} show extra peaks at 1725 cm^{-1} for carbonyl groups as can be seen in Figure 8.

Cation exchange capacity

The CEC of the modified polystyrene films has been determined from the reduction in alkalinity by back titration to be 0.833 mequiv/g, following the procedure given by ASTM standards. This value of CEC compares well with the commercially available membranes and shows that the membrane has become negatively charged on modification.

Contact angle measurement

The contact angle of water on the UM and modified membrane is determined to be 73° and 41°, respectively. The contact angle of water with polystyrene

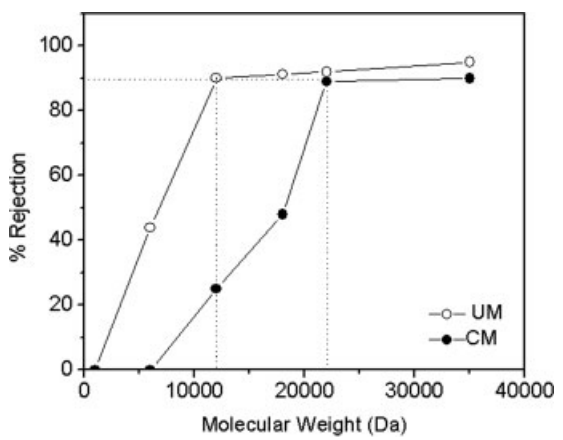

Figure 7 Molecular weight cut off (MWCO) of unmodified (UM) found to 12000 Da (~ 6.0 nm) and carboxylated (CM) 18000 Da (~ 7.8 nm) polystyrene membrane.

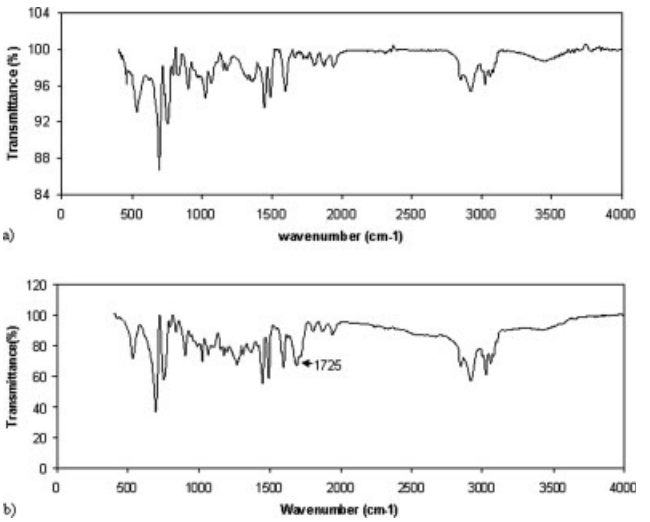

Figure 8 FTIR spectra of (a) unmodified membrane (UM) (b) Carboxylated membrane (CM) where 1725 (cm^{-1}) corresponds to C=O groups.

membrane shows that it is hydrophobic in nature and the decrease in the contact angle on modification indicates that the wettability of the CM has increased on introduction of acid groups on its surface. The increase in hydrophillicity has caused a significant increase in the pure water flux of the modified membranes.

Equilibrium water content

The swelling behavior of the membranes has been investigated in terms of the water content which is estimated to be 1 and 31.2% for the UM and modified polystyrene membrane, respectively. The water content of the modified membrane is considerably higher as compared with the UM because of the presence of acid functional groups on its surface.

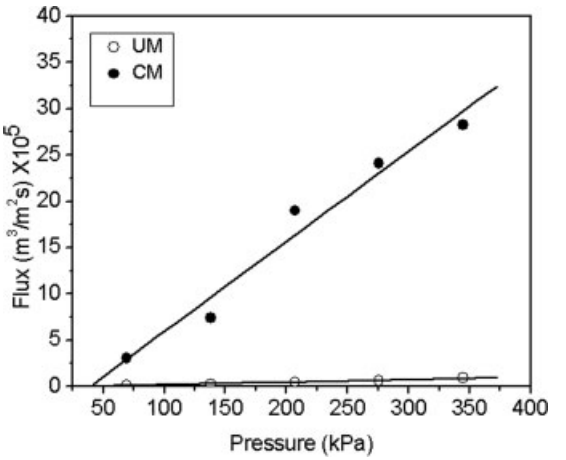

Figure 9 Water flux of unmodified polystyrene (UM) and carboxylated (CM) membranes as a function of pressure showing a manifold increase in flux on modification.

TABLE II
Reflection Coefficient, Solute Permeability, and Pure Water Permeability of the PS Membranes

Type of membranes	Reflection coefficient, σ	Solute permeability, P_m (m/s)	Pure water permeability, L_p (ms^{-1} KPa^{-1})
Unmodified PS	0.916	1.246×10^{-6}	2.49×10^{-8}
Carboxylated PS	0.847	1.588×10^{-6}	8.64×10^{-7}

Hydraulic permeability

Experimental data for the hydraulic permeability have been obtained for the UM and CM as shown in Figure 9. The pure water flux varies linearly with pressure drop in accordance with the Darcy's law ($J_v = L_p \Delta P$). From the slope of the plot, we have determined the pure water permeability and found it to be 2.49×10^{-8} ms^{-1} kPa^{-1} for the UM and 8.64×10^{-7} ms^{-1} kPa^{-1} for the CM (see Table II). It is evident from these results that on modification the water flux has increased by an order of magnitude. This increase in water flux can be explained by the enhancement of membrane hydrophilicity and also due to enlargement of the skin pore size as a result of the modification reaction. These effects have already been shown through contact angle measurements and pore size measurements.

Permeate flux and rejection

Effect of pressure

The membranes so prepared have been used for the separation of chromium (VI) salt solution. We have obtained the permeate flux for the UM and the CM as a function of pressure. Figure 10 shows that with increase in applied pressure the permeate flux increased linearly for both the membranes. For the modified membranes, the solute flux is found to be higher than that of the UM due to an increase of the pore size as well as the hydrophilicity generated by modification reactions (carboxylation). Permeate flux is also obtained at different concentrations of chromium (VI) salt solution so as to study the effect of feed concentration on the permeate flux. As is evident from Figure 10, the permeate flux for the low concentration (100 ppm) chromium (VI) salt solution is higher as compared to the 500 ppm and 1000 ppm permeate flux. This shows that at higher concentrations, membrane gets slightly plugged due to concentration polarization. After every experimental run the pure water flux is measured to ensure that there was no flux decline due to partial plugging.

The chromium (VI) salt rejection as a function of pressure drop for the UM and CM is shown in Figure 11. The observed rejection for the UM increases with pressure drop but on modification the trend changes and the rejection falls with pressure. The permeate flux (Fig. 10) is also found to be lower than the pure water flux which implies that the rejection results have to be corrected to include concentration polarization effects. Thus a procedure is developed as outlined in Section 2.9 to find the real rejection to characterize the membrane performance. The concentration of the chromate ions at the surface of the membrane (C_m) is determined indirectly using Ghose et al.'s model. It is found that the chromate concentration on the membrane surface was three to

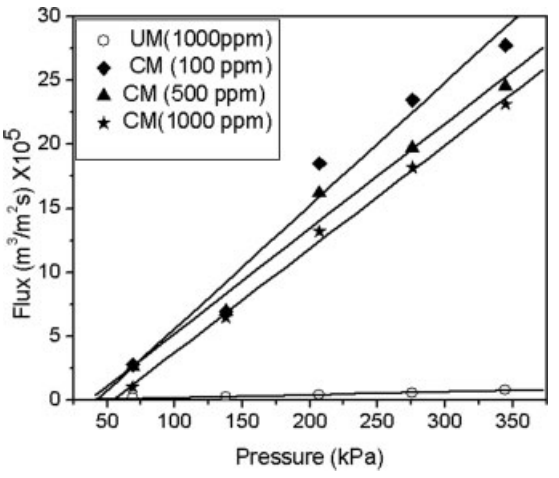

Figure 10 Permeate flux of unmodified PS (UM) and carboxylated PS (CM) membranes as a function of pressure showing a manifold increase in flux on modification. The permeate flux decreased with increase in feed concentration due to concentration polarization.

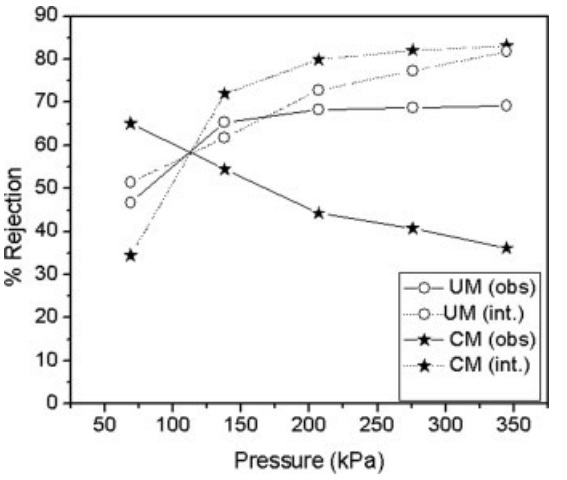

Figure 11 Variation of intrinsic (int.) and observed (obs.) rejection of chromium (VI) salt solution for the unmodified (UM), and carboxylated (CM) PS membranes as a function of pressure (1000 ppm, pH = 3).

four times higher than the concentration in the bulk and there fore the intrinsic (real) rejection always increased with pressure which is also a typical trend of separation of electrolytes from charged membranes. The intrinsic rejection obtained for the CM is around 80% showing a good separation performance for the separation of charged solutes and compares well with the UM. Moreover, CM has much higher permeate flux as compared with the UM. Thus, the chemical modification of the UM causes a manifold increase in the flux with no loss in rejection. The reflection coefficient, σ and the solute permeability, P_m are calculated using the Spiegler-Kedem equation with the best fit of the rejection, R and the permeate flux, J_v and the results are shown in Table II. The reflection coefficient of CM is found to be lower because of the increasing pore size due to the modification reaction. The same arguments hold for the increase in the permeability.

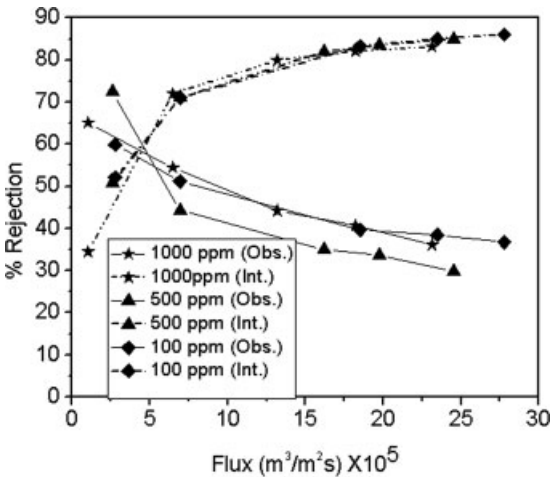

Figure 12 Variation of intrinsic (int.) and observed (obs.) rejection of chromium (VI) salt solution with permeate flux for the carboxylated PS membrane (CM) as a function of feed.

Effect of feed concentration

Rejection data of chromium (VI) salt solutions at different feed concentrations was obtained. The experiments were conducted for the concentration of 1000 ppm, 500 ppm, and 100 ppm for the CM as shown in Figure 12. It was found that the intrinsic rejection increased (though slightly) with the decrease in concentration as has been reported in literature.[45] This is mainly because the effect of Donnan exclusion reduces with the increase in concentration of the electrolyte. In the case of higher electrolyte concentration, the membrane charge is shielded resulting in a lower effective charge of the membrane and hence lower retention.

Analysis using space charge model

In this work, we have analyzed our results based on the model proposed by Sasidhar et al.[42] We have fitted the experimental data ($Pe_p^{\exp}$ and $Pe^{\exp}$ to calculate the concentration at the interface of the membrane (including the rise in bulk concentration due concentration polarization) and the wall potential which are difficult to measure directly. The model requires characteristic membrane structural (pore diameter, membrane area, and pore length) parameters for fitting of the experimental results. The pore diameter, effective membrane area, and pore length (which is the same as membrane thickness) are experimentally known to be 7.8 nm, 36 cm^2, and 30 μm [measured from SEM picture Fig. 4(c)], respectively. The SCM is known to work in the region of large pore size and low concentrations and is consistent with the fact that our membrane is charged ultrafiltration type. In our model, we have assumed the whole system to be divided into two regions where in the first region (Region I), increase in concentration occurs from c_b to c_I due to the unstirred polarization layer and the interfacial resistance of the membrane and in the region II (which corresponds to the membrane capillaries) the SCM holds well and describes the effect of wall potential on the movement of ions. To check the efficiency of our procedure, we have performed the simulation on Pentium IV PC using MATLAB 7.1 software. The tolerance value for the numerical calculation of the solution of Poisson-Boltzmann equation was kept at 10^{-6}. The analysis presented in this work determines the wall potential of this region (region II) and the concentration at the membrane surface (c_I). To show that the series solution reduces the computational load drastically, we determined CPU time required as a function of wall potential and λ. For a typical simulation with the same initial values of pore size and wall potential, the time taken for series solution method is about 15 min as compared to 15 h taken for the MATLAB 7.1 ordinary differential equation solver for the numerical integration. We have presented a semianalytical series solution for the Poisson-Boltzmann equation and in Figure 13 it is shown that the series solution used by us matches completely with the numerical solution of Poisson-Boltzman Equation.

To obtain the dependency of retention on the pore size and wall potential, we have carried out a sensitivity analysis keeping the pressure at a fixed value. In Figure 14, we have shown the effect of change in pore size (1–10 nm) for a fixed value of average wall charge (−28.07 mV) on the retention of chromium (VI) salt solution. It can be seen that for each pressure the rejection increases with increase in pore size though the change is small. Therefore, we can conclude that rejection is almost insensitive to variation

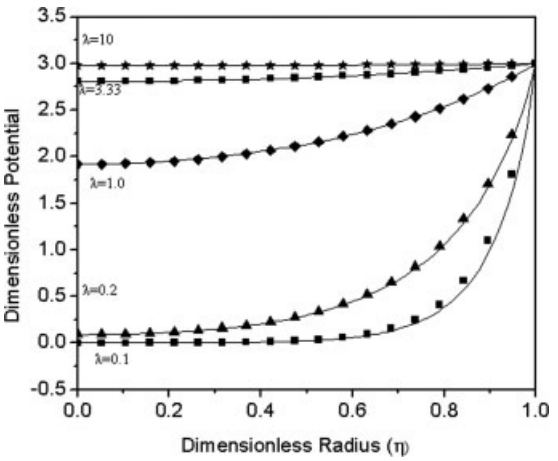

Figure 13 Radial potential distribution inside the capillary at wall potential $\psi_w = 3$ for series solution (dots) and numerical (lines) solution of Poisson-Boltzmann Equation.

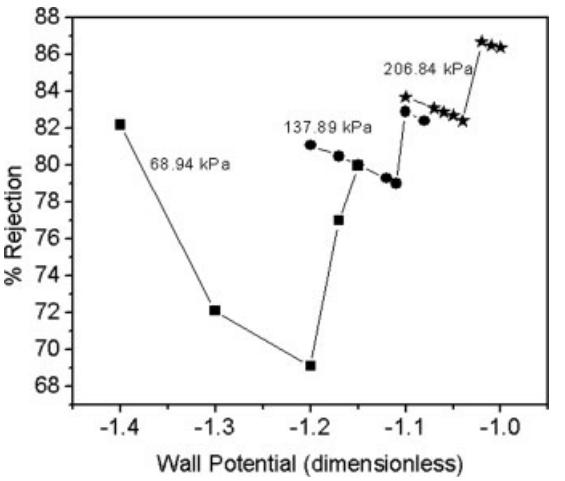

Figure 15 Variation of rejection for different pore wall potential at a fixed pore radius (3.9 nm).

in pore size. Similarly, to check the sensitivity of retention on wall potential, we have varied the wall potential for a fixed value of pore size (obtained from MWCO $\sim$ 3.9 nm). From Figure 15, we find that for each pressure the wall potential undergoes a minimum. Hence, the procedure outlined here for the determination of optimum wall potential is appropriate for the system used in this study.

Using the SCM, we have calculated the wall potential of the CM corresponding to each pressure for three different concentrations at which the experimental data was obtained following the procedure described in Figure 3. The wall potential obtained for each value of pressure is given in Table III. The average wall potential for the charged membranes has been found to be −28.07 mV. The value of wall potential obtained shows that the modified membrane has a low charge density as has also been seen by the ion exchange capacity results. As a result of fitting the experimental results to the SCM, we have obtained the values of surface concentration c_I and hence calculated the rejection for each concentration. In Figure 16, we have compared the rejection of chromium (VI) salt solution obtained using the SCM and the observed rejection at different feed concentrations (1000 ppm, 500 ppm, and 100 ppm). In contrast to the Ghose et al. model which calculates membrane surface concentration by including concentration polarization effects for uncharged solutes, the SCM takes into account the membrane charge as well. The latter model considers osmotic pressure as well as the electrical body force for the calculation of rejection of solute whereas the former takes only osmotic pressure into account for the estimation of rejection.

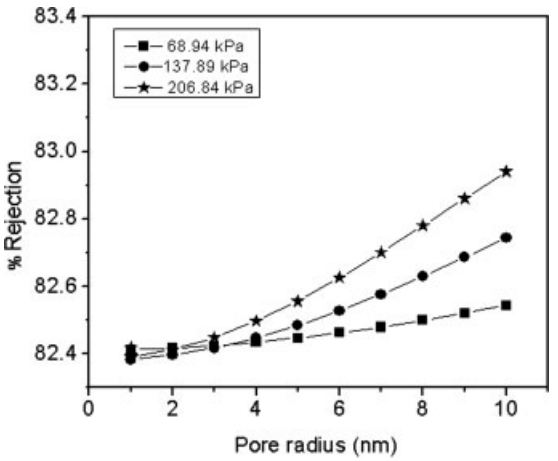

Figure 14 Variation of rejection for different pore radius at a fixed wall potential (−28.07 mV).

CONCLUSIONS

In this work, we have prepared a modified crosslinked ultrafiltration poly (styrene-*co*-divinyl benzene) composite membrane and used it for the separation of chromium (VI) ions. This composite membrane has been prepared by first preparing polymer syrup of styrene/DVB using a dual initiator system (AIBN, BPO and DMA) and subsequently spreading

TABLE III
Wall Potential Values Obtained for Various Pressures and Feed Concentration Carboxylated PS Membranes Using Space Charge Model

Pressure (KPa)	Wall potential (mV) 1000 ppm	Wall potential (mV) 500 ppm	Wall potential (mV) 100 ppm
68.94	−30.03	−30.05	−27.47
137.89	−28.4	−35.17	−27.2
206.84	−27.2	−25.6	−25.6
275.79	−25.9	−25.6	−25.6
344.73	−25.9	−25.6	−25.9

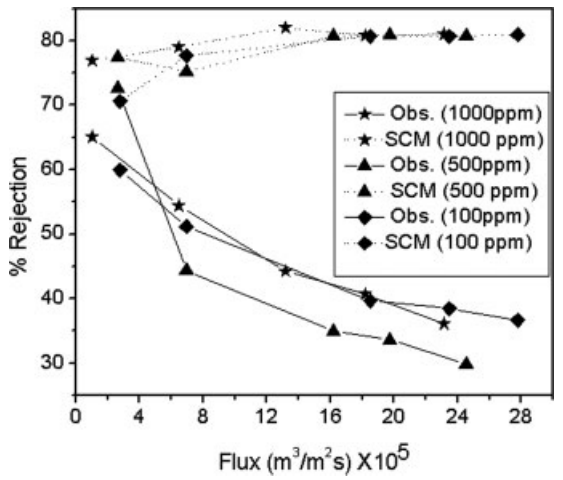

Figure 16 Variation of chromium (VI) salt solution rejection with permeate flux calculated from Space Charge Model (SCM) and observed rejection (Obs.) for the carboxylated PS membrane (CM) as a function feed concentration (pH = 3).

it on a clay support. The membrane so prepared is homogeneously charged by reaction with chloroacetic acid. The chemical modification imparts acid functional groups to the membrane surface making it negatively charged and hydrophilic in nature. The intrinsic rejection coefficient of the membrane has been studied to determine the effect of pressure and concentration of feed solution. It has been found that after modification the membrane becomes highly hydrophilic and very high water flux could be obtained for low values of pressure drop and without much loss of retention of chromium (VI). The intrinsic rejection always increases with pressure even though the trends obtained for observed rejection are much different. Observed and intrinsic rejection data for different concentrations of chromium (VI) salt solution is obtained which shows a slight decrease in solute rejection with increase in feed concentration. The membrane works best at lower concentration as the effect of membrane charge becomes effective and hence higher rejection of the electrolyte is obtained. Finally, the Space Charge model has been used to determine the effective wall potential for the effect of pressure and concentration. The average wall potential for the CM has been found to be −28.07 mV.

NOMENCLATURE

a	Pore radius, m
l	Length of pore, m
A	Area of the cross section of the pore, m^2
c	Concentration of the electrolyte moles/m^3
c_I	Concentration in the polarization layer, moles/m^3
c_p	Concentration in the permeate, moles/m^3
$\overline{c}$	Dimensionless concentration of the electrolyte, c/c_{II}
D_i	Diffusion coefficient of the ith ion, m^2/s
d	Ratio of diffusion coefficients
I	Electrical current through the pore, A
I^*	Dimensionless current through the pores
F	Faradays constant, Coulomb/mol
$j_{+,,x}$	Flux of the ith ion in the axial direction, moles/m^2/s
$j_{+,,r}$	Flux of the ith ion in the radial direction, moles/m^2/s
J	Total solute flux rate across the pore, moles/s
J_w	Pure water flux, m/s
J_s	Average solute flux across the pore moles/s
J_s^*	Dimensionless solute flux
k_i	The integral defines by table A2
L_i	Coefficients defined by eq. (A8)
P	Pressure, N/m^2
Pe	Peclet number: dimensionless average velocity through the pore
Pe_p	Pressure Peclet number
Pe_π	Osmotic pressure Peclet number
$\Re$	Gas constant
T	Absolute Temperature, K
U	Average velocity, m/s
u_x	Axial velocity, m/s
u_r	Radial velocity, m/s
Q	Volumetric flow rate, m^3/s
Y	Dimensionless solvent pressure
z_i	Valency of the ith ion
R_m	Intrinsic hydraulic resistance
L_p	Hydraulic permeability

Greek letters

ε	Dielectric constant
μ	Viscosity of the medium, Poise
μ_w	viscosity of water, Poise
λ_D	Debye length, cm
σ	Surface charge density of the pores of the wall, C/m^2
ξ	Dimensionless axial position, x/l
ω	Dimensionless parameter defined by $4a^2RTc(x)/\ \mu D_+$
λ	Dimensionless debye length, λ_D/a
Φ	Total electrostatic potential, V
ϕ	Axial component of potential, V
$\overline{\phi}$	Dimensionless potential, $F\phi/RT$
ψ	Electric potential due to double layer, V
$\overline{\psi}$	Dimensionless double layer potential, $F\psi/RT$
Ψ_w	wall potential

Subscripts

I, II	Denotes two regions
i	Denotes the *i*th ion; +, cation and −, anion
s	Solute
w	Wall

APPENDIX A

Physical model and governing equations

The ion flux density are given by the Nernst Planck equation as

$$\left.\begin{aligned} j_{i,x} &= u_x c_i - D_i\frac{\partial c_i}{\partial x} - \frac{D_i}{\Re T} z_i c_i F \frac{\partial \Phi}{\partial x} \quad \text{(a)} \\ j_{i,r} &= u_r c_i - D_i\frac{\partial c_i}{\partial r} - \frac{D_i}{\Re T} z_i c_i F \frac{\partial \Phi}{\partial r} \quad \text{(b)} \end{aligned}\right\} \quad \text{(A1)}$$

The steady state fluid velocity is given by the Navier-Stokes equation

$$\left.\begin{aligned} 0 &\cong -\frac{\partial P}{\partial x} - \left(\sum_i F z_i c_i\right)\frac{\partial \Phi}{\partial x} + \mu\left(\frac{1}{r}\frac{\partial}{\partial r}\left(r\frac{\partial u_x}{\partial r}\right) + \frac{\partial^2 u_x}{\partial x^2}\right) \quad \text{(a)} \\ 0 &\cong -\frac{\partial P}{\partial r} - \left(\sum_i F z_i c_i\right)\frac{\partial \Phi}{\partial r} + \mu\left(\frac{1}{r}\frac{\partial}{\partial r}\left(r\frac{\partial u_r}{\partial r}\right) + \frac{\partial^2 u_r}{\partial x^2}\right) \quad \text{(b)} \end{aligned}\right\} \quad \text{(A2)}$$

The relation between electrical potential and the charge density is given by the Poisson equation.

$$\frac{1}{r}\frac{\partial}{\partial r}\left(r\frac{\partial \Phi}{\partial r}\right) + \frac{\partial^2 \Phi}{\partial x^2} = -\frac{\rho}{\varepsilon} = -\frac{F}{\varepsilon}\sum_i c_i \quad \text{(A3)}$$

$$\frac{1}{\eta}\frac{\partial}{\partial \eta}\left(\eta\frac{\partial \bar{\psi}}{\partial \eta}\right) = \frac{1}{\lambda^2}\sinh(\bar{\psi}) \quad \text{(A4)}$$

TABLE A1
First Eleven Nonzero Coefficients of the Series Solution of the Poisson-Boltzmann Equation

Coefficient	Expression
a_2	$\dfrac{\sinh(a_0)}{(2\lambda)^2}$
a_4	$\dfrac{a_2\cosh(a_0)}{(4\lambda)^2}$
a_6	$\dfrac{a_4\cosh(a_0) + a_2^2\sinh(a_0)/2!}{(6\lambda)^2}$
a_8	$\dfrac{(a_6 + a_2^3/3!)\cosh(a_0) \;+\; a_2 a_4\sinh(a_0)}{(8\lambda)^2}$
a_{10}	$\dfrac{a_8\cosh(a_0) + a_2 a_6\sinh(a_0) + \frac{a_4^2\sinh(a_0)}{2!} + \frac{a_2^2 a_4\cosh(a_0)}{2!} + \frac{a_2^4\sinh(a_0)}{4!}}{(10\lambda)^2}$
a_{12}	$\dfrac{\left(a_{10} + \frac{a_2^2 a_6}{2!} + \frac{a_2^5}{5!} + \frac{a_4^2 a_2}{2!}\right)\cosh(a_0) + \left(a_2 a_8 + \frac{a_2^3 a_4}{3!} + a_4 a_6\right)\sinh(a_0)}{(12\lambda)^2}$
a_{14}	$\dfrac{\left(a_{12} + \frac{a_2^2 a_8}{2!} + \frac{a_2^4 a_4}{4!} + \frac{a_4^3}{3!} + a_2 a_4 a_6\right)\cosh(a_0) + \left(a_2 a_{10} + \frac{a_2^3 a_6}{3!} + \frac{a_6^2}{2!} + \frac{a_2^6}{6!} + a_4 a_8\right)\sinh(a_0)}{(14\lambda)^2}$
a_{16}	$\dfrac{\left(a_{14} + \frac{a_2^2 a_{10}}{2!} + \frac{a_2^4 a_6}{4!} + \frac{a_2^7}{7!} + \frac{a_4^2 a_6}{2!} + \frac{a_6^2 a_2}{2!} + a_2 a_4 a_8\right)\cosh(a_0)}{(16\lambda)^2} + \dfrac{\left(a_2 a_{12} + \frac{a_2^3 a_8}{3!} + \frac{a_2^5 a_4}{5!} + a_4 a_{10} + \frac{a_4^3 a_2}{3!} + a_6 a_8 + \frac{a_2^2 a_4 a_6}{2!}\right)\sinh(a_0)}{(16\lambda)^2}$
a_{18}	$\dfrac{\left(a_{16} + \frac{a_2^2 a_{12}}{2!} + \frac{a_2^4 a_8}{4!} + \frac{a_2^6 a_4}{6!} + \frac{a_4^2 a_8}{2!} + \frac{a_6^2 a_4}{2!} + a_2 a_4 a_{10} + a_2 a_6 a_8 + \frac{a_2^3 a_4 a_6}{3!} + \frac{a_2^3 a_6^2}{2!3!}\right)\cosh(a_0)}{(18\lambda)^2} + \dfrac{\left(a_2 a_{14} + \frac{a_2^3 a_{10}}{3!} + \frac{a_2^5 a_6}{5!} + \frac{a_2^8}{8!} + a_4 a_{12} + \frac{a_4^4}{4!} + a_6 a_{10} + \frac{a_8^2}{2!} + \frac{a_2^2 a_4 a_8}{2!} + \frac{a_2^2 a_6^2}{2!2!} + \frac{a_2^4 a_4^2}{4!2!} + \frac{a_2 a_4^2 a_6}{2!}\right)\sinh(a_0)}{(18\lambda)^2}$
a_{20}	$\dfrac{\left(a_{18} + \frac{a_2^2 a_{10}}{2!} + \frac{a_2^4 a_{14}}{4!} + \frac{a_2^6 a_6}{6!} + \frac{a_2^9}{9!} + \frac{a_4^2 a_{10}}{2!} + \frac{a_4^4 a_2}{4!} + \frac{a_6^3}{3!} + \frac{a_8^2 a_2}{2!} + a_2 a_4 a_{12} + a_2 a_6 a_{10} + \frac{a_2^3 a_4 a_8}{3!} + \frac{a_2^3 a_6^2}{2!3!} + a_4 a_6 a_8\right)\cosh(a_0)}{(20\lambda)^2} + \dfrac{\left(a_2 a_{16} + \frac{a_2^3 a_{12}}{3!} + \frac{a_2^5 a_8}{5!} + \frac{a_2^7 a_4}{7!} + a_4 a_{14} + \frac{a_4^3 a_6}{3!} + a_6 a_{12} + a_8 a_{10} + \frac{a_2^2 a_4 a_{10}}{2!} + \frac{a_2^2 a_6 a_8}{2!} + \frac{a_2 a_4^2 a_8}{2!} + \frac{a_2 a_4 a_6^2}{2!}\right)\sinh(a_0)}{(20\lambda)^2}$

TABLE A2
Expressions for k_i

Integral expression	Analytical solution (using series solution)
$k_0 = \int_0^1 \eta(\bar{\psi} - \bar{\psi}_w)d\eta$	$k_0 = \sum_{i=0}^{\infty} \frac{ia_i}{2(i+2)}$
$k_1 = \int_0^1 \eta\left(\int_\eta^1 \frac{1}{\eta_1}\left(\int_0^{\eta_1} \eta_2 \cosh\bar{\psi}d\eta_2\right)d\eta_1\right)d\eta$	$k_1 = \lambda^2 \sum_{i=0}^{\infty} \frac{b_i}{2(i+2)(i+4)}$
$k_2 = \int_0^1 \eta(1-\eta^2)\sinh(\bar{\psi})d\eta$	$k_2 = \sum_{i=0}^{\infty} \frac{2(i+2)a_{i+2}}{i+4}$
$k_3 = \int_0^1 \eta \sinh\bar{\psi}\left(\int_\eta^1 \frac{1}{\eta_1}\left(\int_0^{\eta_1} \eta_2 \cosh\bar{\psi}d\eta_2\right)d\eta_1\right)d\eta$	$k_3 = \lambda^2 \sum_{i=0}^{\infty} \frac{b_i}{(i+2)^2} \sum_{i=0}^{\infty} (i+2)^2 a_{i+2} - \sum_{i=0}^{\infty}\sum_{j=0}^{i} \frac{(i+2-j)^2 a_{i+2-j} b_j}{(i+4)(j+2)^2}$
$k_4 = \int_0^1 \eta\left(de^{\bar{\psi}} - e^{-\bar{\psi}}\right)d\eta$	$k_4 = \lambda^2(d+1)\sum_{i=0}^{\infty}(i+2)a_{i+2} + \lambda^2(d-1)\sum_{i=0}^{\infty}\frac{b_i}{(i+2)}$
$k_5 = \int_0^1 \eta\left(de^{\bar{\psi}} + e^{-\bar{\psi}}\right)d\eta$	$k_5 = \lambda^2(d-1)\sum_{i=0}^{\infty}(i+2)a_{i+2} + \lambda^2(d+1)\sum_{i=0}^{\infty}\frac{b_i}{(i+2)}$
$k_6 = \int_0^1 \eta(\bar{\psi} - \bar{\psi}_w)\sinh\bar{\psi}d\eta$	$k_6 = \sum_{i=0}^{\infty}\sum_{j=0}^{i}\frac{(i-j+2)^2 a_j a_{i-j+2}}{i+2} - \sum_{i=0}^{\infty} a_i \sum_{i=0}^{\infty}(i+2)a_{i+2}$
$k_7 = \int_0^1 \eta\cosh\bar{\psi}\left(\int_\eta^1 \frac{1}{\eta_1}\left(\int_0^{\eta_1} \eta_2 \cosh\bar{\psi}d\eta_2\right)d\eta_1\right)d\eta$	$k_7 = \lambda^2 \sum_{i=0}^{\infty}\sum_{j=0}^{i}\frac{b_j b_{i-j}}{(i+1)^2(i+1)} + \sum_{i=0}^{\infty}\frac{b_i}{(i+2)^2}\sum_{i=0}^{\infty}\frac{b_i}{i+2}$
$k_8 = \int_0^1 \eta(\bar{\psi} - \bar{\psi}_w)\cosh\bar{\psi}d\eta$	$k_8 = \lambda^2 \sum_{i=0}^{\infty}\sum_{j=0}^{i}\frac{a_j b_{i-j}}{(i+2)} - \lambda^2 \sum_{i=0}^{\infty} a_i \sum_{i=0}^{\infty}\frac{b_i}{i+2}$
$k_9 = \int_0^1 \eta(1-\eta^2)\cosh\bar{\psi}d\eta$	$k_9 = \lambda^2 \sum_{i=0}^{\infty}\frac{2b_i}{(i+2)(i+4)}$

where $\bar{\psi} = \sum_{i=0}^{\infty} a_i\eta^i$ $\sinh(\psi) = \lambda^2 \sum (i+2)^2 a_{i+2}\eta^i$ $\cosh(\psi) = \lambda^2\sum_{i=0}^{\infty}(i+1)(i+3)^2 a_{i+3}\eta^i / \sum_{i=0}^{\infty}(i+3)a_{i+1}\eta^i = \lambda^2 \sum b_i\eta^i$.

where,

$$\bar{\psi} = \frac{F\psi}{\Re T}, \quad \eta = \frac{r}{a} \quad \text{and} \quad \lambda = \frac{\kappa}{a}, \quad \kappa = \left(\frac{\varepsilon \Re T}{2F^2 c(x)}\right)$$

The boundary conditions of the equation are

$$\left.\frac{\partial\bar{\psi}}{\partial\eta}\right|_{\eta=0} = 0 \quad \text{(a)}$$
$$\left.\bar{\psi}\right|_{\eta=1} = \bar{\psi}_w \quad \text{or,} \quad \text{(b)}$$
$$\left.\frac{\partial\bar{\psi}}{\partial\eta}\right|_{\eta=1} = \bar{q} = \frac{Fqa}{\varepsilon RT} \quad \text{(c)} \qquad \text{(A5)}$$

$$Pe\frac{Ul}{D_+} = -\frac{L_3}{\bar{c}}\frac{d\bar{c}}{d\xi} + L_4\frac{dY}{d\xi} \qquad \text{(A6)}$$

$$J_s^* = -L_1\frac{d\bar{c}}{d\xi} + \bar{c}L_2\frac{dY}{d\xi} \qquad \text{(A7)}$$

where Pe is Peclet number,

$$\xi = \frac{x}{l}, \quad \bar{c} = \frac{c(x)}{c_{II}}, \quad \bar{\phi} = \frac{F\phi}{RT}, \quad \omega = \frac{4a^2RTc(x)}{\mu D_+}$$
$$Y = -\frac{a^2}{8\mu D_+}(P-\pi), \quad J_s^* = \frac{J_s l}{D_+ c_{II}}$$

$$L_1 = k_5 + \omega k_7 - \frac{(k_4 - \omega\lambda^2 k_8)(k_4 + \omega k_3)}{(k_5 - \omega\lambda^2 k_6)} \quad \text{(a)}$$
$$L_2 = 4k_9 - 4k_2\frac{(k_4 - \omega\lambda^2 k_8)}{(k_5 - \omega\lambda^2 k_6)} \quad \text{(b)}$$
$$L_3 = \omega k_1 - \omega\lambda^2 k_0\frac{(k_4 + \omega k_3)}{(k_5 - \omega\lambda^2 k_6)} \quad \text{(c)}$$
$$\text{and} \quad L_4 = 1 + \frac{4\omega\lambda^2 k_0 k_2}{(k_5 - \omega\lambda^2 k_6)} \quad \text{(d)} \qquad \text{(A8)}$$

where the k_i's are given in Table A2.

$$Pe = \int_{\bar{c}(\xi=0)}^{\bar{c}(\xi=1)} \left\{\frac{L_2L_3 - L_1L_4}{(J_s^*/Pe)L_4 - \bar{c}L_2}\right\}d\bar{c} \qquad \text{(A9)}$$

$$-\frac{a^2}{8\mu D_+}\left[(P-\Pi)_{\xi=1} - (P-\Pi)_{\xi=0}\right] = \int_{\bar{c}(\xi=0)}^{\bar{c}(\xi=1)} \left\{\frac{(J_s^*/Pe)L_3 - \bar{c}L_1}{(J_s^*/Pe)L_4 - \bar{c}L_2}\right\}\frac{d\bar{c}}{\bar{c}} \qquad \text{(A10)}$$

References

1. Kesting, R. E. Synthetic Polymeric Membranes; Wiley: New York, 1985.
2. Zularisam, A. W.; Ismail, A. F.; Salim, M. R.; Sakinah, M.; Hiroaki, O. J Membr Sci 2007, 299, 97.

3. Chan, R.; Chen, V. J Membr Sci 2004, 242, 169.
4. Susanto, H.; Franzka, S.; Ulbricht, M. J Membr Sci 2007, 296, 147.
5. Koh, M.; Clark, M. M.; Howe, K. J. J Membr Sci 2005, 256, 169.
6. Ríos-Dominguez, H.; Ruiz-Treviño, F. A.; Contreras-Reyes, R.; González-Montiel, A. J Membr Sci 2006, 271, 94.
7. Choi, Y.-J.; Kang, M.-S.; Kim, S.-H.; Cho, J.; Moon, S.-H. J Membr Sci 2003, 223, 201.
8. Gohil, G. S.; Shahi, V. K.; Rangarajan, R. J Membr Sci 2004, 240, 211.
9. Franco, D. R.; Amado, A.; Evandro Gondran, B.; Ferreira, J. Z.; Rodrigues, M. A. S.; Ferreira, C. A. J Membr Sci 2004, 234, 139.
10. Smitha, B.; Sridhar, S.; Khan, A. A. J Membr Sci 2003, 225, 63.
11. Kim, J.; Kim, B.; Jung, B. J Membr Sci 2002, 207, 129.
12. Hosono, T.; Tanioka, A. Polymer 1998, 39, 4199.
13. Eto, R.; Tanioka, A. J Colloid Interface Sci 1998, 200, 59.
14. Brighton, C. A.; Pritchard, G.; Skinner, G. A. Styrene Polymers: Technology and Environmental Aspects; Applied Science Publishers: London, 1979.
15. Nagarale, R. K.; Gohil, G. S.; Shahi, V. K.; Rangarajan, R. Colloids and Surf A Physicochem. Eng Aspects 2004, 251, 133.
16. Nemes, S.; Borbely, J.; Borda, J.; Kelen, T. Polym Bull 1991, 27, 123.
17. Sukhishvili, S. A.; Chechik, O. S.; Yaroslavov, A. A. J Colloid Interface Sci 1996, 178, 42.
18. Richard, F. C.; Bourg, A. C. Water Res 1991, 25, 807.
19. Kroschwitz, J. L. Kirk-Othmer Encyclopedia of Chemical Technology; Wiley: New York, 1991.
20. de Souza E Silva, P. T.; de Mello, N. T., Menezes Duarte, M. M.; Montenegro, M. C.; Araújo, A. N.; de Barros Neto, B.; da Silva, V. L. J Hazard Mater 2006, B128, 39.
21. Rengaraj, S.; Yeon, K.-H.; Moon, S.-H. J Hazard Mater 2001, B87, 273.
22. Tenorio, J. A. S.; Espinosa, D. C. R. Waste Manage 2001, 21, 637.
23. Frenzel, I.; Stamatialis, D. F.; Wessling, M. Sep Purif Technol 2006, 49, 76.
24. Baral, S. S.; Das, S. N.; Rath, P. Biochem Eng J 2006, 31, 216.
25. Noro, J.; Maruyana, K.; Komatsu, Y. Anal Sci 2001, 17, 1333.
26. Lanagan, M. D.; Ibana, D. C. Miner Eng 2003, 16, 237.
27. Schaffer, A. I.; Fane, A. G.; Waite, T. D. Nanofiltration-Principles and Applications; Elsevier: New York, 2005.
28. Cassano, A.; Drioli, E.; Molinari, R.; Bertolutti, C. Desalination 1996, 108, 193.
29. Hafez, A. I.; El-Manharawy, M. S.; Kehdre, M. A. Desalination 2002, 144, 237.
30. Hafiane, A.; Lemordant, D.; Dhahbi, M. Desalination 2005, 130, 305.
31. Shukla, A.; Kumar, A. J Membr Sci 2004, 237, 119.
32. Neelakandan, C.; Pugazhenthi, G.; Kumar, A. Eur Polymer J 2003, 39, 2383.
33. Pugazhenthi, G.; Sachan, S.; Kishore, N.; Kumar, A. J Membr Sci 2005, 254, 229.
34. Gues, E. R.; den Exter, M. J.; Bekkum, H. V. J Chem Soc Faraday Trans 1992, 88, 3101.
35. Singh, S.; Khulbe, K. C.; Matsuura, T.; Ramamurthy, P. J Membr Sci 1998, 142, 111.
36. IS: 7330-1988, Indian Standard, Methods of sampling and test for ion-exchange resins (first revision) 1989, p 1–14.
37. Mahlab, D.; Yosef, N. B.; Belfort, G. Chem Eng Commun 1980, 226, 225.
38. Clifton, M. Polarization de concentration dans divers procedes de separation a membrane; These, Universite Paul Sabatier, Toulhouse: France, 1982.
39. Vilker, V. L.; Colton, C. K.; Smith, K. A. AIChE J 1981, 27, 632.
40. Spiegler, K. S.; Kedem, O. Desalination 1966, 1, 311.
41. Ghose, S.; Bhattacharjee, C.; Datta, S. J Membr Sci 2000, 169, 29.
42. Sasidhar, V.; Ruckenstein, E. J Colloid Interface Sci 1981, 82, 439.
43. Coury, L. Curr Separations 1999, 18, 91.
44. Elvy, S. B.; Dennis, G. R.; Ng, L.-T. J Appl Polym Sci 1995, 56, 591.
45. Peeters, J. M. M.; Boom, J. P.; Mulder, M. H. V.; Strathmann, H. J Membr Sci 1998, 145, 199.